Investigation on the electrocatalytic oxidation of alcohol using zinc oxide thin films deposited by pulsed electrodeposition on an indium tin oxide surface

M. Lakhdari

Laboratoire d'électrochimie et matériaux, Faculté de Technologie.
Département de génie des procédés, Université Ferhat Abbas Sétif-1, 19000 Sétif, Algérie.

K. Hadj Larbi

Laboratoire d'électrochimie et matériaux, Faculté de Technologie,
Département de génie des procédés, Université Ferhat Abbas Sétif-1, 19000 Sétif, Algérie.

A. Nebatti Ech-chergui

Laboratory of Materials and Applications, University Centre Belhadj Bouchaib of Ain-Temouchent,
Ain Temouchent, Algeria.

F. Habelhames

Laboratoire d'électrochimie et matériaux (LEM), Faculté de Technologie,
Département de génie des procédés, Université Ferhat Abbas Sétif-1, 19000 Sétif, Algérie.

N. Benaioun

Laboratory of Theory and Simulation of Materials, Faculty of Exact and Applied Sciences,
University of Oran1, Ahmed Ben Bella, Oran, Algeria.

J. Michel Nunzi

Department of Chemistry, Queen's University, Kingston, ON K7L 3N6, Canada,
Department of Physics, Engineering Physics and Astronomy, Queen's University, Kingston, ON K7L 3N6, Canada.

S. Kumar Mukherjee

Department of Physics, Birla Institute of Technology, Mesra, Ranchi - 835215.

M. Adjdir

Applied Organic Synthesis Laboratory, Department of Chemistry, Faculty of Science, University of Oran,
BP 1524, El Menaouar Oran, 31000, Algeria.

Received 13 January 2023; accepted 11 June 2023

To perform electro-catalytic oxidation of alcohols in an alkaline media, zinc oxide (ZnO) thin films were effectively deposited on indium tin oxide (ITO) substrates using the pulsed electrodeposition (PE) method in a zinc nitrate aqueous solution. Analyses of microstructural, photoelectrochemical, and optical characteristics of ZnO thin films were performed as a function of pulsed electrodeposition parameters. XRD analysis was applied to determine structural properties, and SEM and AFM analysis were used to investigate morphological characteristics. X-ray diffraction analyses revealed that the produced films were polycrystalline and had a (002) preferentially oriented, hexagonal wurtzite structure. The morphology of ZnO has improved in the direction of nanorod films, as evidenced by scanning electron microscopy (SEM) and atomic force microscopy (AFM) images. UV transmittance data was used using Tauc's relationship to determine the film's bandgap to be 3.26 eV. The photocurrent response shows that ZnO films have high values, at 305.17 A/cm^2, and good optical characteristics. The electrocatalytic oxidation of methanol was finally evaluated on the films. After being optimized in the pulsed electrodeposition mode, ZnO thin film characteristics and methanol electrocatalytic oxidation both saw substantial improvements.

Keywords: Zinc oxide; pulsed electrodeposition; electrocatalytic oxidation; alcohols.

DOI: https://doi.org/10.31349/RevMexFis.70.011005

1. Introduction

Our current reliance on fossil fuels for energy generation can lead to significant ecological and economic issues. The use of renewable energy sources could help mitigate [1]. Fuel cells are one option because of their potential to turn chemical energy into electrical energy with minimal damage to the environment [2].

There are currently numerous types of fuel cells in use [2–4]. Methanol and ethanol are used as chemical fuels in direct alcohol fuel cells, which have been hailed as a promising renewable energy technology. It is supported by scholarly

evidence [5] that the direct oxidation of alcohols has various benefits, including increased efficiency, a wider range of viable electrode materials, and reduced interference from the oxidation of other organic fuels. Methanol offers many advantages over ethanol, including being cheaper overall, having a higher energy density, being readily available from multiple sources, and being easy to store and transport. Since alcohols play such a crucial role in direct alcohol fuel cells, research into their electrochemical oxidation has received a lot of attention [6]. The primary difficulty is finding a suitable replacement for the expensive platinum and palladium alloys currently used in alkaline batteries. There has been significant work toward developing highly active electrocatalysts for alcohols [5] by employing metal oxides as support systems for catalytic metal sites, such as TiO_2 [7], MnO_2 [8], $NiCO_2O_4$ [9], etc.

Zinc oxide (ZnO) is a notable nontoxic n-type semiconductor with a wide direct band gap at the ambient temperature of 3.37 eV because of its chemical stability as well as its electrical and optical features, such as n-type conductivity and a wide range of visual transmittance. This is because ZnO has a wide range of visual transmittance [10]. Solar cells [11], sensors [12], batteries [13], smart windows [14], photocatalysts [15], etc., all make use of ZnO to varying degrees. Sputtering [16], chemical vapor deposition [17, 18], sol-gel using a spin coating or dip coating procedure [19, 20], electrodeposition [21], hydrothermal growth [22, 23], and spray pyrolysis [24] are only some of the methods that have been used to create ZnO thin films. Since it is straightforward, inexpensive, and can potentially be used for massive industrial production, the electrodeposition method stands out as a crucial and straightforward technology for the creation of thin films. In addition, in comparison to other methods, this one offers a number of advantages, the most notable of which is its low processing temperature, its adaptability in terms of substrate geometry, and its manageable film thickness [25]. Studies on modifying the morphology of electrodeposit-formed ZnO films have been conducted on multiple occasions [26]. Electrodeposition potential [27], annealing temperature [28], and growth rate [29] are just a few of the parameters that may be changed to produce a variety of morphologies. Particularly, it has been shown that pulsed electrodeposition (PE) encourages the nucleation and organization of small crystals [30] and improves attributes like porosity [31], ductility [32], hardness [33], and surface roughness [34]. Therefore, it should be feasible to optimize films for any desired morphology and attributes by adjusting the deposition settings.

Using a technique known as pulsed-pulse electrodeposition, a modified ZnO film electrode was created for the purpose of investigating electrocatalytic oxidation. It's also worth noting that, to the best of our knowledge, no prior work has been done on the oxidation of methanol to determine the electrocatalytic oxidation of ZnO films using a process similar to the one we used.

2. Experimental

The ZnO thin films employed in the electrocatalytic oxidation of alcohols were synthesized using a pulsed electrodeposition (PE) method. Electrodeposition was carried out in a solution containing 0.1 M Zinc Nitrate (Zn (NO3)2: Sigma-Aldrich) as the Zn2+ source, 5.5 starting pH of deionized water and a synthesis temperature of $80 \pm 1^{\circ}$C.

The conventional three-electrode cell was used to carry out the pulsed electrodeposition procedure. For the electrodes, we employed 2.2 cm^2 of sputtered glass coated with indium tin oxide (ITO), a platinum mesh counter electrode, and a saturated calomel electrode (SCE) as the reference. Films were electrodeposited, then washed in deionized water, then annealed at 400°C for 1 h, with a $5^{\circ}\text{C}\cdot\text{min}^{-1}$ heating rate.

The acquired footage is analyzed using a number of various analysis techniques. To create the electrodeposition, a Voltalab PGZ 301 potentiostat-galvanostat was used. The crystal structure of the samples was confirmed by X-ray diffraction (XRD) using a CuK radiation ($\lambda = 1.5406$ Å) Bruker D8 Advance diffractometer fitted with a linear Vantec super speed detector. Scanning Electron Microscopy (SEM) was used to examine the surface morphology at 10.00 KV. Quantitative atomic force microscopy (AFM) measurements were taken to delve deeper into the morphology's finer points. Using a Shimadzu UV-1800 spectrophotometer, we measured the samples' optical transmittance in the range of 200 to 1200 nm. In 0.1 M K_2SO_4 electrolyte, photocurrent was measured using a monochromatic UV-lamp at $\lambda = 365$ nm. To investigate electrochemical methanol oxidation, a ZnO/ITO (2.2 cm^2 in the geometric area) working electrode was used. As a counter electrode, a platinum wire was employed, and as a reference electrode, a saturated calomel electrode (SCE) was put to good use. The conventional three configuration of an electrochemical quartz cell was used in this experiment. CV measurements were taken during electrochemical oxidation with a potentiostat/galvanostat (Voltalab PGZ 301) throughout a 0-1 V potential range. The NaOH content in the starting solution was 0.1 M, and the amount of methanol was variable.

3. Results and discussion

3.1. Film preparation

ZnO thin film pulsed electrodeposition (PE) curves onto ITO at two potentials are depicted in Fig. 1. The deposition potential is -1.1 V vs. SCE for the time-on (t_{on}) portion of each pulse. during the time-off (t_{off}) phase, an open-circuit potential ($OCP = +0.27$ V vs. SCE) is applied. The on-time for deposition was set at 5 s and the off time was set at 1 s.

Whenever the time-on potential is applied, a negatively charged layer is created around the substrate (ITO) in PE. This layer thickens to a predefined threshold, blocking access

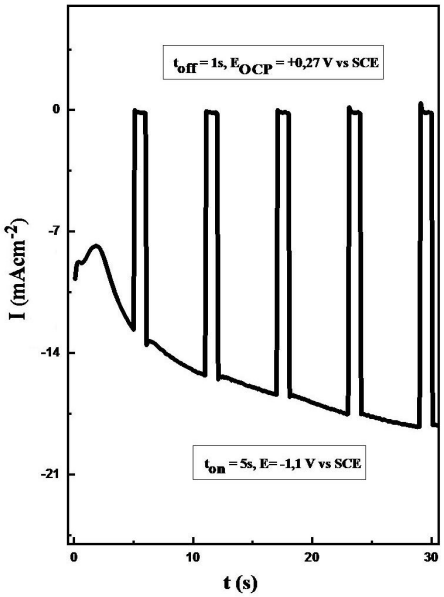

FIGURE 1. Pulsed electrodeposition of ZnO thin films for the first five cycles in a 0.1 M $Zn(NO_3)_2$ solution ($t_{on} = 5$ s, $t_{off} = 1$ s).

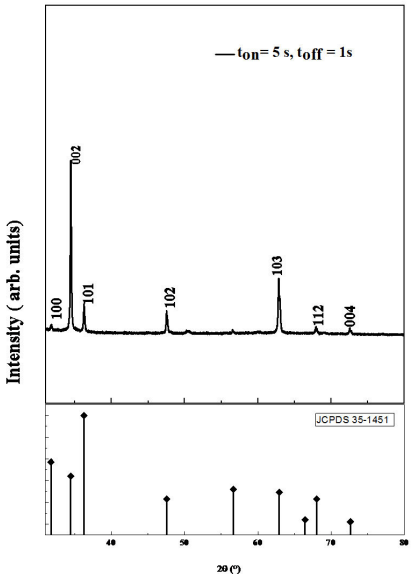

FIGURE 2. XRD patterns of ZnO thin films deposited by PE ($t_{on} = 5$ s, $t_{off} = 1$ s)

to the substrate for the ions. This generated layer is then discharged under the time-off potential (OCP). So, the ions can more easily penetrate the layer and reach the substrate underneath. During time Off, the bath's ions move to a deprived area. After a short delay, the pulse is turned on again, and this time there are more uniformly dispersed ions available for deposition into the substrate [35].

3.2. Crystalline structure

ZnO thin films deposited through pulsed electrodeposition on ITO glass substrates are shown as XRD patterns in Fig. 2. All the patterns' peaks correspond well to the hexagonal wurtzite type (JCPDS $35-1451$), with (002) being the preferred orientation of ZnO. It is well known that the growth of ZnO crystallites along the c-axis is congruent with the enhancement in (002) reflection, measured in terms of relative intensity [36]. Narrow diffraction peaks show and hint at the good crystalline quality of the deposited films [37].

The crystallite sizes 'D' of the films were calculated by the well-known Debye-Scherrer equation

$$D = \frac{k\lambda}{\beta \cos\theta}, \tag{1}$$

$$a = \frac{\lambda}{\sqrt{3}\sin\theta'}, \tag{2}$$

$$c = \frac{\lambda}{\sin\theta(hkl)}, \tag{3}$$

$$V = 0.886 \times a^2 \times c, \tag{4}$$

$$2d_{(hkl)} \sin\theta = n\lambda, \tag{5}$$

where a and c lattice parameters, the volume of the lattice, $d_{(hkl)}$ is the interplanar spacing, D is the crystallite size in nm, ($\lambda = 1.5406$) is the wavelength of CuKα radiation, k is the shape factor, β is the full-width half maximum (FWHM) intensity and $d_{(hkl)}$ is the interplanar spacing. The lattice parameters a and c calculated from the diffractograms are found to be less than those typically seen for undoped ZnO ($a = 3.249$ and $c = 5.207$) [1] as shown in Table I, as well as the volume of the lattice ($V = 47.62$ Å) [1]. This difference is significant and may be due to several factors [2,3]. The grain size of the ZnO thin films prepared by PE is 90.65 nm. In addition, our film has a crystal orientation preference and a high (002) peak intensity. To improve this finding, we must determine the preferential orientation by calculating the texture coefficients using Eq. (8). Observe that the texture coefficient of the (002) plane (TC (002)) is greater than TC (103), indicating that the (002) peak is now preferentially oriented.

TABLE I. Calculated structural parameters for ZnO electrodeposited by EP.

sample	PE
2θ(Å)	34.58
β	0.1827
d(Å)	2.591
c(Å)	5.183
a(Å)	2.992
V(Å^3)	41.10
D (nm)	90.65
Dislocation Density (δ) (10^{-3}line/m^2)	0.73
Tc(002)	1.289
Tc(103)	0.763
Strain(ϵ)(10^{-3})	0.93

Furthermore, strain (ϵ) and dislocation density (δ) were calculated using Eqs. (6) and (7), and the values are presented in Table I.

$$\epsilon = \frac{\beta \cos\theta}{4}, \tag{6}$$

$$a = \frac{1}{D^2}, \tag{7}$$

$$TC_{hkl} = \frac{\frac{(I_{(hkl)})}{I_0(hkl)}}{\sum \frac{(I_{(hkl)})}{I_0(hkl)}}, \tag{8}$$

where $I(hkl)$ and $I_0(hkl)$ denote the measured intensity and the intensity of the standard powder diffraction pattern, respectively, and N is the number of considered reflections.

3.3. Morphological characterizations (SEM and AFM)

Scanning electron microscopy was used to examine the films' morphology after deposition (SEM). In Fig. 3a) and b) display the SEM picture b). The results of pulsed electrodeposition ($t_{on} = 5$ s, $t_{off} = 1$ s) show that the ZnO nanostructures are spread evenly across the ITO surface, with hexagonal nanorods and some nanosheets of significant size having formed. However, it is observed that as the nanosheets assemble into longer blooms, their density decreases. Atomic force microscopy better revealed the ZnO growth in 2D and 3D directions (AFM). Figure 4 displays the results of the AFM analysis of ZnO thin films. Figure 4a) and b) display ZnO thin films with a surface topography consisting of uniformly sized and distributed hexagonal structures. The rms roughness of the films before oxidation is 11.9 nm and after oxidation, it is 22.6 nm. As shown in Fig. 4, the maximum roughness of a few ZnO sites reaches high values. Due to the rarity of these locations, however, their impact is greatly diminished when represented as rms roughness. Figure 5a) shows an AFM image showing the ZnO layer pre-oxidation, showing that it is produced by vast domains. After oxidation, as seen in Fig. 5b), oxide grains form on the ZnO layer's surface, leading to an increase in RMS roughness.

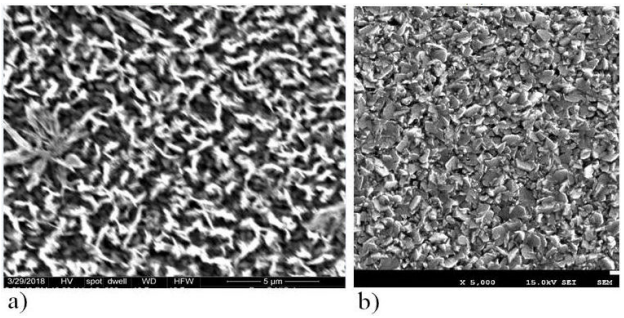

FIGURE 3. SEM image of ZnO thin films deposited by PE ($t_{on} = 5$ s, $t_{off} = 1$ s) a) before oxidation, b) after oxidation.

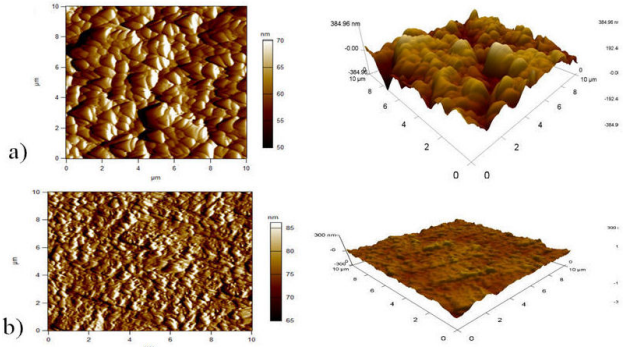

FIGURE 4. AFM surface images (10×10 μm^2) of ZnO thin films deposited by PE ($t_{on} = 5$ s, $t_{off} = 1$ s) a) before oxidation, b) after oxidation.

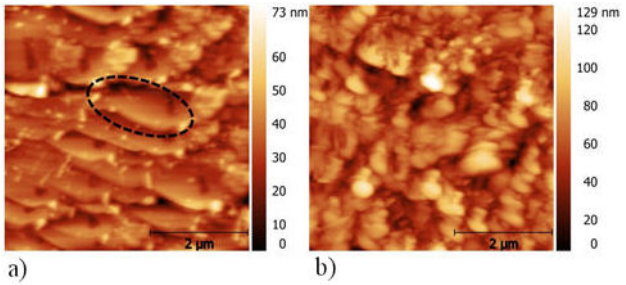

FIGURE 5. AFM surface images (5×5 μm^2) of ZnO thin films deposited by PE ($t_{on} = 5$ s, $t_{off} = 1$ s) a) before oxidation ($RMS = 11.9$ nm), b) after oxidation ($RMS = 22.6$ nm).

3.4. Optical properties

As a function of wavelength, the optical transmittance curves are displayed in Fig. 6a). In the range of 300-900 nm, researchers measured the optical transmittance spectra of pure ZnO. The transmittance of the ZnO film is around 53%. AFM micrographs show that the growth of ZnO crystallites has become more uniform in both its repartition and orientation, which accounts for the higher value. Indeed, it has been reported that the films are suitable candidates as transparent conductive oxide (TCO) for electrochemical and photoelectrochemical (PEC) applications since the optical transparency greatly depends on the surface irregularity and crystallinity of the films.

The optical band gaps of the samples were calculated from the transmission data using the Tauc equation is given as follows:

$$\alpha(h\upsilon) = B(h\upsilon - E_g), \tag{9}$$

where α, h, υ, B, and E_g respectively define the absorption coefficient, the Planck constant, the frequency, a constant, and the band gap. A straight band gap exists in ZnO. Figure 6 depicts the transmission spectrum and the band gap obtained by extrapolating the plot of $(\alpha h\upsilon)^2$ vs. h (Tauc's relationship) to the x-axis (b). So, the film had a band gap of roughly 3.26 eV. Our results for ZnO thin films correlate well with those found in the literature [38].

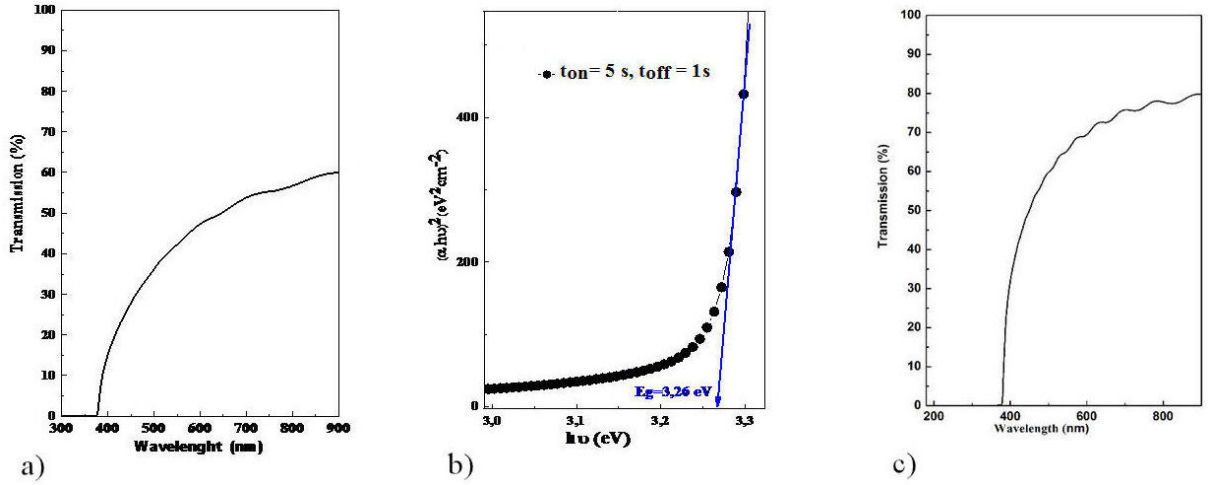

FIGURE 6. Optical transmittance a) and the estimation of band gap b) of ZnO thin films deposited by PE ($t_{on} = 5$ s, $t_{off} = 1$ s) c) ZnO films after oxidation.

After oxidation, the transmittance of ZnO films increases dramatically to 70% at 600 nm, and their absorption edge shifts to longer wavelengths, indicating a slight reduction in the band gap. It is the increased catalytic oxidation of the surface layer of the film during oxidation that causes the increase in transmittance. The shrinkage of the grain size during catalytic oxidation may account for the decrease in the band gap.

3.5. Photoelectrochemical (PEC) properties

A photoelectrochemical analysis was performed to determine the conduction type of ZnO, as described above. The photocurrent responses of ZnO films are shown in Fig. 7 under 5-second ON-OFF cycles of UV light. The films were deposited at times of 5 s and 1 s. Under light, ZnO films exhibit an anodic (positive) current, revealing their n-type semiconductor conductivity [39–41]. Photo-responses were measured to be 305.17 A·cm^{-2} for ZnO films deposited at $t_{on} = 5$ s, $t_{off} = 1$ s when exposed to a constant potential of $+0.8$ V.

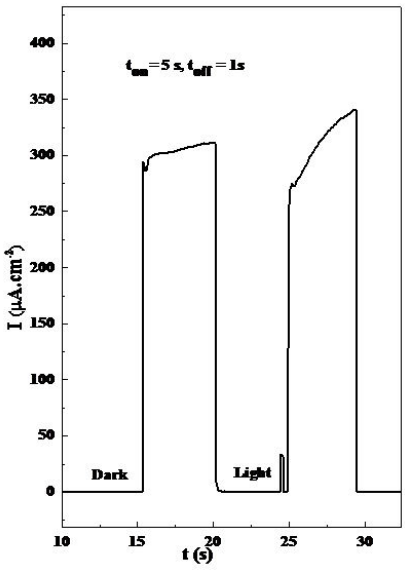

FIGURE 7. Photocurrent responses of ZnO thin films deposited by PE ($t_{on} = 5$ s, $t_{off} = 1$ s).

3.6. Electrocatalytic oxidation of alcohols

Using cyclic voltammetry in 0.1 M NaOH with an organic molecule of methanol, ZnO thin films were deposited onto an ITO substrate from a solution of 0.1 M $Zn(NO_3)_2$ for pulsed electrodeposition time-On value of 450 s. This allowed for an investigation of the ZnO's electrochemical behavior in basic media.

The ITO substrate was electrochemically silent in the potential range of interest, as evidenced by the lack of any appreciable current at the surface of the ITO electrode in the presence of organic molecules [Fig. 8a)]. In addition, no appreciable current is measured at an ITO electrode when the organic molecules are present, suggesting that the ITO substrate lacks electrocatalytic activity for the oxidation of these compounds. The oxygen evolution reaction is shown to begin at a potential of 650 mV in the absence of alcohols [Fig. 8b), curve 1], and to increase toward a more positive potential of 700 mV in the presence of organic molecules [Fig. 8b)], curves 2, 3, and 4).

The irreversible oxidation of alcohol is reflected as a single oxidation peak at the ZnO electrode. Rapidly increasing over time, the methanol oxidation current reaches its maximum at a voltage of around 580 mV. ZnO thin films produce an anodic current [Fig. 8b), curve 1] that is much lower than the currents obtained in solutions containing organic molecules [Fig. 8b), curves 2, 3, and 4]. The anodic current and the potential value of the oxidation peak in the anodic direction both rise with increasing alcohol volume. Since more molecules will be oxidized on the ZnO thin films as the volume increases, the oxidation current will also rise.

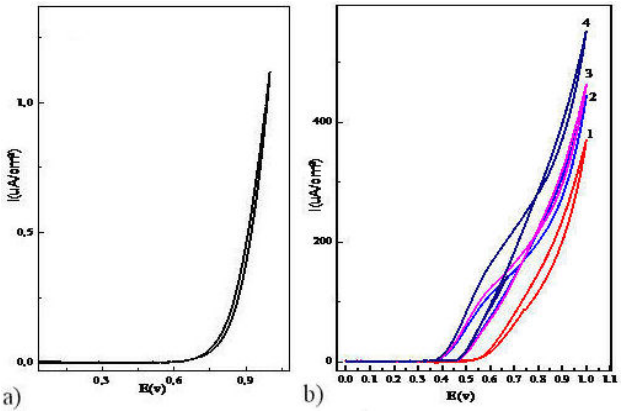

FIGURE 8. a) is the cyclic voltammograms in 0.1 M NaOH of ITO in the presence of alcohols. Figure 8b) presents cyclic voltammograms of ZnO thin Films in 0.1 M NaOH in the absence of methanol (1) and the presence of differences volumes of methanol 1 mL (2); 2 mL (3) and 3 mL (4).

4. Conclusion

To produce ZnO thin films on an ITO substrate using pulsed electrodeposition (PE), it was necessary to optimize the conditions based on the data presented in this contribution. Produced ZnO films possessed a wurtzite structure with a pronounced orientation preference (002). Because the films exhibit large photogenerated currents when exposed to light, the process of pulsed electrodeposition offers potential as a way for preparing expensive window material for electrochemical and photoelectrochemical cells. This is because of the nature of the films. In light of the findings that were obtained, it was determined that the electrocatalytic oxidation of methanol could be performed with the assistance of zinc oxide that had been produced through the technique of pulsed electrodeposition.

Acknowledgment

Our thanks go to Professor Jean Michel Nunzi of Queen's University, Canada's Department of Chemistry, Department of Physics, and Department of Engineering Physics and Astronomy for his insightful conversations and the direction they provided. This study was conducted with funding from Belhadj Bouchaib Ain-Temouchenet University as part of PRFU Project N B00L02UN460120220001.

Declarations Conflict of interest

The authors declare no competing financial interest

Data availability statement

The data that support the findings of this study are available from the corresponding author, upon reasonable request.

1. B. Dunn, H. Kamath, And J.-M. Tarascon, Electrical energy storage for the grid: a battery of choices. *Science*, **334** (2011) 928-935. https://doi.org/10.1126/science.1212741

2. C. Bianchini, And P. K. Shen, Palladium-based electrocatalysts for alcohol oxidation in half cells and in direct alcohol fuel cells. *Chemical reviews*, **109** (2009) 4183-4206. https://doi.org/10.1021/cr9000995

3. M. K. Debe, Electrocatalyst approaches and challenges for automotive fuel cells. *Nature*, **486** (2012) 43-51. https://doi.org/10.1038/nature11115

4. A. Brouzgou, S. Q. Song, and Tsiakaras, Low and non-platinum electrocatalysts for PEMFCs: Current status, challenges and prospects. *Applied Catalysis B: Environmental*, **127** (2012) 371-388. https://doi.org/10.1016/j.apcatb.2012.08.031

5. L. P. R. Profeti, *et al.*, Application of $Pt + RuO_2$ catalysts prepared by thermal decomposition of polymeric precursors to DMFC. *Journal of Power Sources*, **158** (2006) 1195-1201. https://doi.org/10.1016/j.jpowsour.2005.09.061

6. T. Gunji, *et al.*, Facile route for the preparation of ordered intermetallic Pt_3Pb-$PtPb$ core-shell nanoparticles and its enhanced activity for alkaline methanol and ethanol oxidation. *Journal of Power Sources*, **273** (2015) 990-998. https://doi.org/10.1016/j.jpowsour.2014.09.182

7. W. Zhuang, *et al.*, TiO_2 nanofibers heterogeneously wrapped with reduced graphene oxide as efficient Pt electrocatalyst supports for methanol oxidation. *International Journal of Hydrogen Energy*, **40** (2015) 3679-3688. https://doi.org/10.1016/j.ijhydene.2015.01.042

8. R. M. A. Hameed, *et al.*, Promotion effect of manganese oxide on the electrocatalytic activity of Pt/C for methanol oxidation in acid medium. *Applied Surface Science*, **359** (2015) 651-663. https://doi.org/10.1016/j.apsusc.2015.10.130

9. R. Ding, *et al.*, Simple hydrothermal synthesis of mesoporous spinel $NiCO_2O_4$ nanoparticles and their catalytic behavior in CH_3OH electro-oxidation and H_2O_2 electro-reduction. *Catalysis Science & Technology*, **3** (2013) 3207-3215. https://doi.org/10.1039/C3CY00590A

10. N. A. Abdullah, Z. Khusaimi, and M. Rusop, A review on zinc oxide nanostructures: Doping and gas sensing. *Advanced Materials Research*, **667** (2013) 329-332. https://doi.org/10.4028/www.scientific.net/AMR.667.329

11. B. U. Ian YY. Novel all solution processed heterojunction using p-type cupric oxide and n-type zinc oxide nanowires for solar cell applications. *Ceramics International*,

39 (2013) 8073-8078. https://doi.org/10.1016/j.ceramint.2013.03.079

12. A. Nebatti, C. Pflitsch, and B. Atakan, Unusual application of aluminium-doped ZnO thin film developed by metalorganic chemical vapour deposition for surface temperature sensor. *Thin Solid Films,* **636** (2017) 532-536. https://doi.org/10.1016/j.tsf.2017.07.002

13. Q. Tan, *et al.,* Crystallization of zinc oxide quantum dots on graphene sheets as an anode material for lithium ion batteries. *Cryst. Eng. Comm,* **22** (2020) 320-329. https://doi.org/10.1039/C9CE01285K

14. I. Shtepliuk *et al.,* Excitonic emission in heavily Ga-doped zinc oxide films grown on GaN. *Journal of Luminescence*, **223** (2020) 117265. https://doi.org/10.1016/j.jlumin.2020.117265

15. K. Flores *et al.,* The effect of hybrid zinc oxide/graphene oxide (ZnO/GO) nano-catalysts on the photocatalytic degradation of simazine. *Chemosphere*, **259** (2020) 127414. https://doi.org/10.1016/j.chemosphere.2020.127414

16. T. K. Subramanyam, B. Srinivasulu Naidu, and S. Uthanna, Physical properties of zinc oxide films prepared by dc reactive magnetron sputtering at different sputtering pressures. Crystal Research and Technology: *Journal of Experimental and Industrial Crystallography*, **35** (2000) 1193-1202. https://doi.org/10.1002/1521-4079(200010)35:10⟨1193::AID-CRAT1193⟩3.0.CO;2-6

17. C. Pflitsch *et al.,* MOCVD-growth of thin zinc oxide films from zinc acetylacetonate and air. *Journal of crystal growth*, **348** (2012) 5-9. https://doi.org/10.1016/j.jcrysgro.2012.03.016

18. A. E. Nebatti *et al.,* Rapid thermal (RT) MOCVD of undoped and Al doped ZnO thin films. *ECS Transactions,* **25** (2009) 459. https://doi.org/10.1149/1.3207626

19. K. Sadek *et al.,* Structural, Chemical and Optical Properties of Pure and Al-Doped Zno Thin Films Derived by Sol-Gel Dip Coating Process. *Annals of West University of Timisoara-Physics,* **63** (2021) 57-71. https://doi.org/10.2478/awutp-2021-0005

20. G. Soman, *et al.,* Structural and optical studies of zinc oxide thin films prepared via sol-gel spin coating method. In: AIP Conference Proceedings. (AIP Publishing, 2020). https://doi.org/10.1063/5.0017275

21. S. Yang *et al.,* Electrodeposition of hierarchical zinc oxide nanostructures on metal meshes as photoanodes for flexible dye-sensitized solar cells. Colloids and Surfaces A: *Physicochemical and Engineering Aspects*, **594** (2020) 124665. https://doi.org/10.1016/j.colsurfa.2020.124665

22. Q. Liu *et al.,* Ammonia-induced seed layer transformations in a hydrothermal growth process of zinc oxide nanowires. *The Journal of Physical Chemistry C*, **124** (2020) 20563-20568. https://doi.org/10.1021/acs.jpcc.0c05490

23. A. Sadek Kadari *et al.,* Atomic mapping of Li: ZnO thin films and its spectroscopic analysis. *Inorganic Chemistry Communications,* **132** (2021) 108852. https://doi.org/10.1016/j.inoche.2021.108852

24. S. Kurtaran Al doped ZnO thin films obtained by spray pyrolysis technique: influence of different annealing time. *Optical Materials*, **114** (2021) 110908. https://doi.org/10.1016/j.optmat.2021.110908

25. H. Chettah, And D. Abdi, Effect of the electrochemical technique on nanocrystalline ZnO electrodeposition, its structural, morphological and photoelectrochemical properties. *Thin Solid Films*, **537** (2013) 119-123. https://doi.org/10.1016/j.tsf.2013.04.024

26. A. Arslan *et al.,* Controlled growth of c-axis oriented ZnO nanorod array films by electrodeposition method and characterization. *Spectrochimica Acta Part A: Molecular and Biomolecular Spectroscopy*, **128** (2014) 716-723. https://doi.org/10.1016/j.saa.2014.02.123

27. V. Manzano *et al.,* ZnO morphology control by pulsed electrodeposition. *The Journal of Physical Chemistry C*, **117** (2013) 1502-1508. https://doi.org/10.1021/jp3107099

28. S.-S. Xu *et al.,* Bandgap narrowing and conductivity evolution of atomic-layer-deposited ZnO: Cu thin films under rapid thermal annealing. *Journal of Alloys and Compounds*, **638** (2015) 133-135. https://doi.org/10.1016/j.jallcom.2015.03.083

29. Y. Robin *et al.,* Influence of the growth rate on the morphology of electrodeposited zinc oxide. *Superlattices and Microstructures*, **73** (2014) 281-289. https://doi.org/10.1016/j.spmi.2014.05.032

30. J. Xue, *et al.,* The study on formation mechanism of novel ZnO cone prepared by using pulsed current electrodeposition. *Materials Letters*, **125** (2014) 99-102. https://doi.org/10.1016/j.matlet.2014.03.139

31. K. I. Popov, D. N. Keča, and M. D. Andjelič, Electrodeposition of zinc on copper from alkaline zincate solutions. *Journal of Applied Electrochemistry,* **8** (1978) 19-23. https://doi.org/10.1007/BF00615389

32. Ch. J. Raub, and A. Knödler, The electrodeposition of gold by pulse plating: Improvements in the properties of deposits. *Gold Bulletin,* **10** (1977) 38-44. https://doi.org/10.1007/BF03215426

33. Kh. M. S. Youssef,, C. C. Koch, And S. Fedkiw Improved corrosion behavior of nanocrystalline zinc produced by pulse-current electrodeposition. *Corrosion Science,* **46** (2004) 51-64. http://dx.doi.org/10.1016/S0010-938X(03)00142-2

34. R. G. A. Garcia *et al.,* Antimony sulfide (Sb_2S_3) thin films by pulse electrodeposition: Effect of thermal treatment on structural, optical and electrical properties. *Materials Science in Semiconductor Processing,* **44** (2016) 91-100. https://doi.org/10.1016/j.mssp.2015.12.018

35. M. Lakhdari, *et al.,* Effects of pulsed electrodeposition parameters on the properties of zinc oxide thin films to improve the photoelectrochemical and photoelectrodegradation efficiency. *The European Physical Journal Applied Physics*, **84** (2018) 30102. https://doi.org/10.1051/epjap/2018180227

36. J. B. Wang, *et al.,* Erratum: Raman scattering and high temperature ferromagnetism of Mn-doped ZnO nanoparticles [*Appl. Phys. Lett.* **88** (2006) 252502]. *Applied Physics Letters*, (2006) 89 https://doi.org/10.1063/1.2234562

37. B. Abderrahmane *et al.*, Improvement of ZnO nanorods photoelectrochemical, optical, structural and morphological characterizations by cerium ions doping. *Journal of Alloys and Compounds*, **829** (2020) 154498. https://doi.org/10.1016/j.jallcom.2020.154498

38. E. Sarica, and V. Bilgin, Structural, optical, electrical and magnetic studies of ultrasonically sprayed ZnO thin films doped with vanadium. *Surface and Coatings Technology*, **286** (2016) 1-8. https://doi.org/10.1016/j.surfcoat.2015.12.008

39. J.-J. Kim, *et al.*, Characteristics of laser-annealed ZnO thin film transistors. *Thin Solid Films*, **518** (2010) 3022-3025. https://doi.org/10.1016/j.tsf.2009.09.190

40. M. Lakhdari, and F. Habelhames, Morphological and structural control of pulse electrodeposited ZnO thin films and its influence on the photoelectrocatalytic degradation of methyl orange. *Journal of Materials Science: Materials in Electronics*, **30** (2019) 6107-6115. https://doi.org/10.1007/s10854-019-00912-1

41. K.H. Larbi *et al.*, A comparative study of a direct and pulse electrode-position method of TiO_2 films and its effect on photo-electrocatalytic degradation of methyl orange dye. *Optoelectron. Lett.* **17** (2021) 334-341. https://doi.org/10.1007/s11801-021-0193-4